Fabrication of arbitrarily shaped silicon and silicon oxide nanostructures using tip-based nanofabrication

Huan Hu, Parsian K. Mohseni, Lei Pan, Xiuling Li, Suhas Somnath, Jonathan R. Felts, Mark A. Shannon, and William P. King

Fabrication of arbitrarily shaped silicon and silicon oxide nanostructures using tip-based nanofabrication

Huan Hu, Parsian K. Mohseni, Lei Pan, and Xiuling Li
Department of Electrical and Computer Engineering, University of Illinois at Urbana-Champaign, Urbana, Illinois 61801

Suhas Somnath, Jonathan R. Felts, Mark A. Shannon, and William P. King[a]
Department of Mechanical Science and Engineering, University of Illinois at Urbana-Champaign, Urbana, Illinois 61801

The authors report fabrication of arbitrary shapes of silicon and silicon oxide nanostructures using tip-based nanofabrication (TBN). A heated atomic force microscope (AFM) tip deposits molten polymer on a substrate to form polymer nanostructures that serve as etch mask to fabricate silicon or silicon oxide nanostructures. The authors demonstrate how TBN can be combined with conventional wet etching as well as metal-assisted chemical etching, in order to fabricate these nanostructures. The size of the TBN-fabricated silicon nanostructures is around 200 nm. Silicon nanostructures fabricated using metal-assisted chemical etch can have very smooth sidewalls with, roughness as small as 2 nm. The authors show fabrication of arbitrary shapes of silicon and silicon oxide nanostructures including those with curved and circular shapes. Our results show that TBN using a heated AFM tip can function as an additive nanolithography technique with minimum contamination, and is compatible with existing nanofabrication methods. © *2013 American Vacuum Society*. [http://dx.doi.org/10.1116/1.4831767]

I. INTRODUCTION

Tip-based nanofabrication (TBN) uses a nanometer-scale tip to interact with a sample to fabricate nanostructures. TBN has the potential for fabricating nanostructures with controlled size, shape, and orientation at precise substrate locations and nanometer-scale precision and resolution.[1] In TBN, a tip can interact with the sample to fabricate nanostructures, with the tip influencing the surface through any of a number of mechanisms, including mechanical,[2] electrochemical,[3] optical,[4] chemical diffusion,[5] thermal,[6] electrical polarization,[7] and plasma.[8]

Although TBN has many advantages, there are only a few published articles that describe the use of TBN for nanodevice fabrication.[9–16] A key challenge to realizing TBN-fabricated nanodevices is to incorporate TBN fabrication steps with other processing steps. Unfortunately, most TBN methods are not easily compatible with nanofabrication.[17–22] For example, dip pen nanolithography (DPN) can fabricate silicon nanostructures only when combined with intermediate chemical processing steps. One publication showed the use of DPN to fabricate gold nanostructures using DPN, and then used these gold nanostructures as a masking step for subsequent etching.[23] Oxidation-based TBN can fabricate silicon oxide nanostructures with only a few nanometers in thickness due to the slow oxidation rate. One publication showed that the oxidation rate falls dramatically due to self-limiting behavior resulting from the build-up stress and a reduction of electrical field strength.[24] To achieve device fabrication using TBN, a key challenge is improved compatibility with silicon fabrication processes.

Here, we show that a heated AFM tip can deposit thick polymer nanostructures and transfer the written structures into both silicon and silicon oxide films in a one-step etching process. Moreover, we show the flexibility of the technique by demonstrating the fabrication of arbitrary shapes of solid structures of silicon oxide. Our TBN method is compatible with existing nanofabrication methods and especially suitable for device fabrication.

II. EXPERIMENTAL AND RESULTS

A. Nanostructures formed using tip-based nanofabrication and wet chemical etching

Figure 1 shows the process used to fabricate silicon oxide nanostructures by TBN. First, we grew a 50 nm thick silicon oxide layer via thermal oxidation at 1000 °C for 80 min. Then, a heated AFM tip deposited polystyrene (PS) on top of the oxide layer via TBN. Following polymer deposition, we etched the 50 nm thick silicon oxide layer by dipping the sample into buffered hydrofluoric acid (BHF) for 60 s. BHF etched the silicon oxide that was not masked by the PS nanopatterns. The last step was to remove PS by acetone and oxygen plasma reactive ion etching (RIE).

A key step in the process is to provide polymer ink onto the cantilever tip and to then deliver the polymer ink onto the surface. The polymer was loaded onto the cantilever tip by bringing the heated AFM tip end onto a PS fiber. The heated tip melted the PS, and then the PS flowed onto the tip.[25] After inking, we mounted the tip in an Asylum Research MFP-3D AFM and scanned the tip along a programmed path with a constant force at a speed of 150 nm/s.[25] A closed-loop feedback circuit maintained the cantilever heater temperature at 260 °C.[26] When the tip was
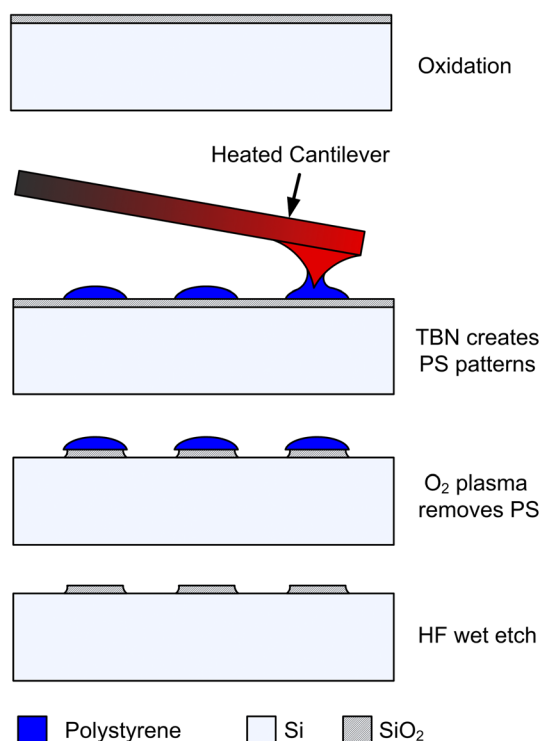

FIG. 1. (Color online) Schematics showing process for fabricating silicon oxide nanostructures via TBN. The tip deposits molten polymer onto silicon oxide. The polymer nanostructures serve as an etch mask.
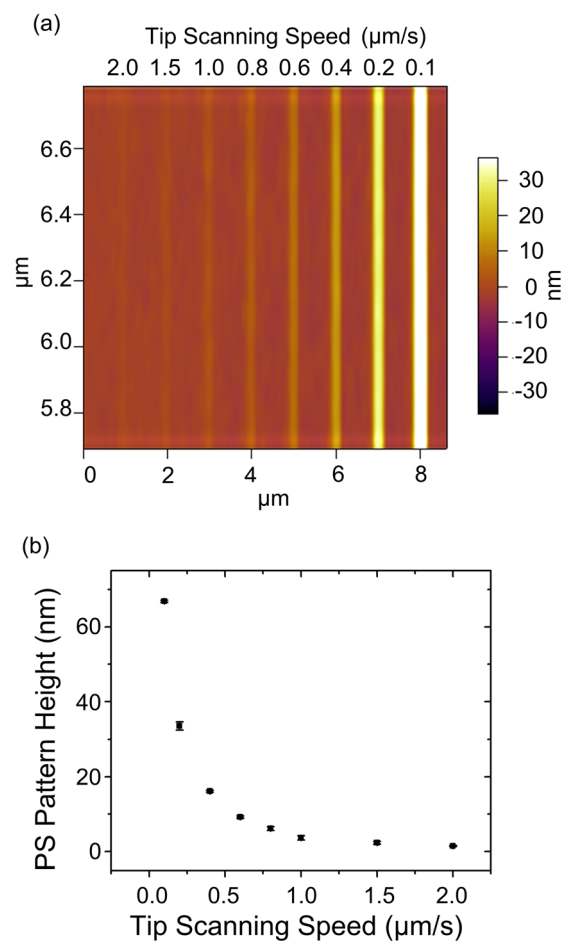

FIG. 2. (Color online) (a) AFM topography of linear PS nanopatterns deposited by the heated AFM tip at different tip scanning speeds as shown. (b) Summary of PS nanopattern heights at different tip scanning speeds.

hot, the molten polymer would flow from the moving tip to the substrate and form solid PS nanostructures.[6] The force between the tip and the substrate was maintained around 200 nN during the deposition. During heating, the tip-sample adhesion force, measured by pulling the tip off of the surface, was about 425 nN.

Figure 2(a) shows an AFM contact mode image of various PS linear nanostructures deposited using the heated AFM tip at different tip scanning speeds. The PS linear nanostructures from right to left as shown in Fig. 2(a) are deposited by the heated AFM tip at 0.1, 0.2, 0.4, 0.6, 0.8, 1.0, 1.5, and 2.0 μm/s tip scanning speeds. Figure 2(b) summarizes the PS nanostructures heights at different tip scanning speeds. As the tip scanning speed increases, the deposited polymer lines are thinner. This is consistent with a previous publication, which showed that polymer deposition rate is relatively independent from tip speed.[25] Thus, a faster moving tip deposits less amount of polymer per unit length and therefore produces a thinner line.

Figure 3(a) shows a scanning electron microscope (SEM) image of silicon oxide nanostructures fabricated by TBN at different writing speeds from 0.1 to 2 μm/s. Figure 3(b) shows AFM tapping mode image of the silicon oxide nanostructures. Figure 3(c) summarizes the silicon oxide nanostructure height versus the tip writing speed. All three figures show that silicon oxide nanostructures fabricated at slow tip writing speeds are taller than at those fabricated at fast tip writing speeds. The slower tip speeds correspond with thicker polymer structures on the surface, which better protect the silicon oxide during etching. As shown in Fig. 3,

when the tip speed exceeds 0.6 μm/s, the silicon oxide nanostructures become discontinuous. To fabricate unbroken silicon oxide nanostructures, the tip writing speed should be less than 0.6 μm/s. To ensure good quality silicon oxide nanostructures, we choose the tip writing speed to be 150 nm/s for all the experiments, with the exception of the dot-writing experiments, where the tip was stationary.

Figure 4(a) shows SEM images of two sets of circular silicon oxide nanostructures fabricated by TBN. In this case, the masking layer was TBN-fabricated PS nanodots, which served as the mask for hydrofluoric acid (HF) etching of the silicon oxide layer. The polymer nanodots were deposited by a stationary heated tip with dwelling times from 2 to 16 s with an incremental step of 2 s. Figure 4(b) shows an AFM tapping mode image of a single oxide dot pattern fabricated by dwelling the tip for 4 s and followed by BHF etching. The indentation on the circular silicon oxide nanostructure was formed because of the indentation of its etching mask, the molten polymer nanodot. When the heated AFM tip finished depositing the polymer nanostructure, the heating was turned off. The indentation on the nanostructure was formed during polymer cooling with the tip still in contact with the polymer deposit. Figure 4(c) summarizes how the tip dwelling time impacts the size of
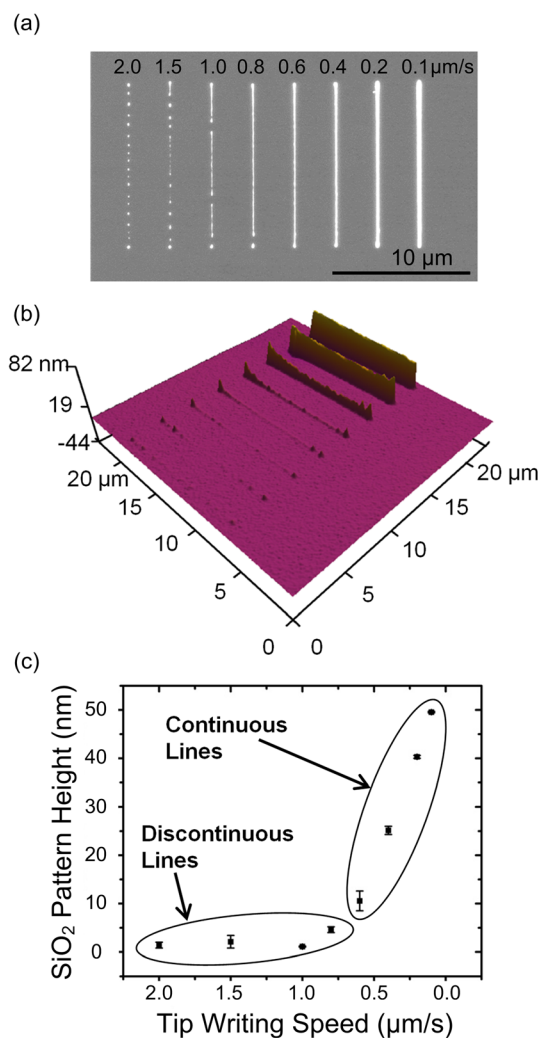
FIG. 3. (Color online) (a) SEM image of silicon oxide nanostructures fabricated via BHF wet etch. The PS nanostructures were deposited at different tip speeds, and served as an etch mask. (b) AFM tapping mode image of the silicon oxide structures. (c) Silicon oxide nanostructure height vs tip writing speeds. When tip writing speed is above 600 nm/s, silicon oxide nanostructures are no longer continuous.
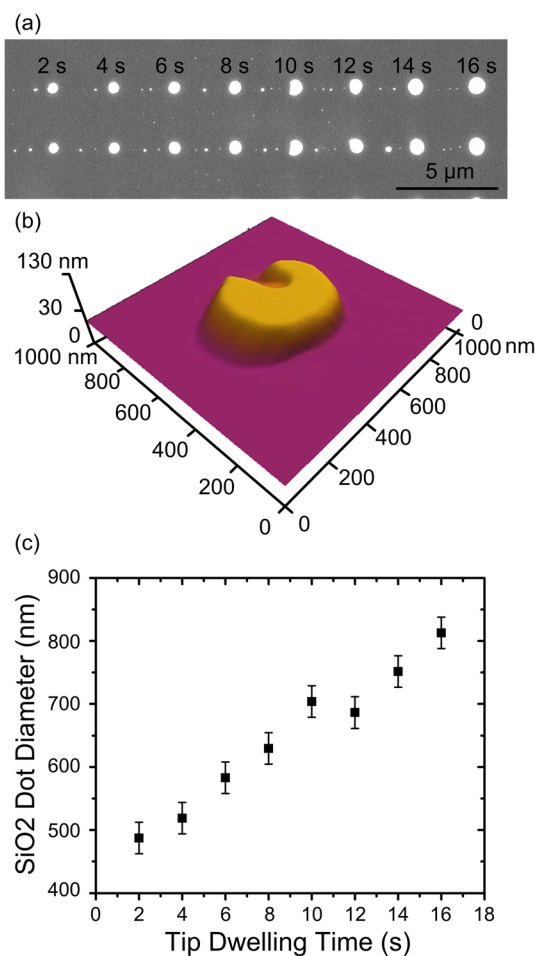

FIG. 4. (Color online) (a) SEM image of two sets of circular silicon oxide nanostructures fabricated using different tip dwelling times. (b) AFM tapping mode topography image of a circular silicon oxide nanostructure fabricated by TBN. The dwelling time was 4 s for the nanostructure. (c) Diameter of the circular silicon oxide nanostructures as a function of tip dwelling times.

the circular silicon oxide nanostructures. The diameter of the circular silicon oxide nanostructure increases with the incremental increase of the tip dwelling time, which is consistent with previous publications.[27]

Figure 5 shows SEM images of various basic silicon oxide nanostructures fabricated using the process described in Fig. 1. All the structures are 50 nm in height. Figures 5(a) and 5(b) show an array of silicon oxide fin structures, each fin is 20 μm in length and 250 nm in width. Figures 5(c) and 5(d) show an array of curved silicon oxide fins structures. Each curved fin structure is consisting of a series of short linear fin structures. The heated AFM tip dwells longer in the joints between two short linear lines and, therefore, results in thicker nodes as shown in Figs. 5(c) and 5(d). Figures 5(e) and 5(f) show an array of 8 × 8 circular silicon oxide nanostructures and each circular nanostructure is about 250 nm in diameter.

Figure 6 shows SEM images of various complex shapes of silicon oxide structures fabricated using the process

described in Fig. 1. Figures 6(a) and 6(b) show a circular ring silicon oxide structure with a diameter of 7.8 μm. The ring consists of 32 individual line segments. Figure 6(c) shows a series of silicon oxide nanostructures mimicking ancient Chinese characters. Figure 6(d) shows the zoomed-in view of one character. Figures 6(e) and 6(f) show a lotus flower structure. The difference in the width of the pattern is due to different tip dwelling times. The tip dwells longer in the joints between two lines and, therefore, results in thicker patterns. All the above images demonstrate that our TBN method can fabricate arbitrary patterns of PS and transfer the patterns to solid silicon oxide structures. Since wet etching is an isotropic process, resulting in undercutting, the PS nanopatterns cannot mask the silicon oxide that is thicker than the width of the PS nanopatterns.

B. Nanostructures formed using tip-based nanofabrication and metal-assisted chemical etching

Figure 7 shows our process to fabricate nanostructures using TBN and metal-assisted chemical etching (MacEtch).[27,28] First,
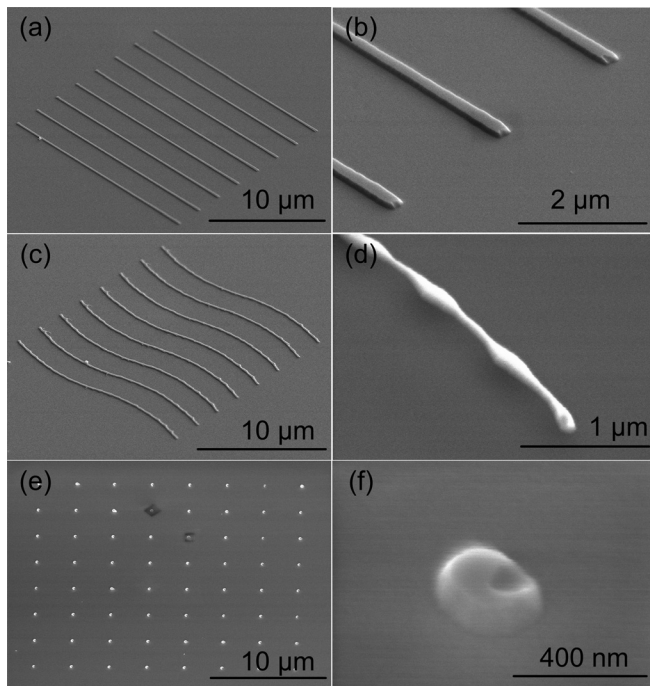
FIG. 5. SEM images of basic types of silicon oxide nanostructures fabricated via TBN. (a) Array of silicon oxide fin structures, each fin is 20 μm long and 250 nm wide. (b) Zoomed-in view of silicon oxide fin structure. (c) Array of eight curved silicon oxide fins. The curved fin consists of a series of linear fins. (d) Zoomed-in view of a section of a single curved fin. The thicker region joins between two adjacent linear fins where the heated tip paused. (e) Array of silicon oxide circular nanostructures, where each circular nanostructure is about 250 nm in diameter. (f) Zoomed-in view of a single circular silicon oxide nanostructure.
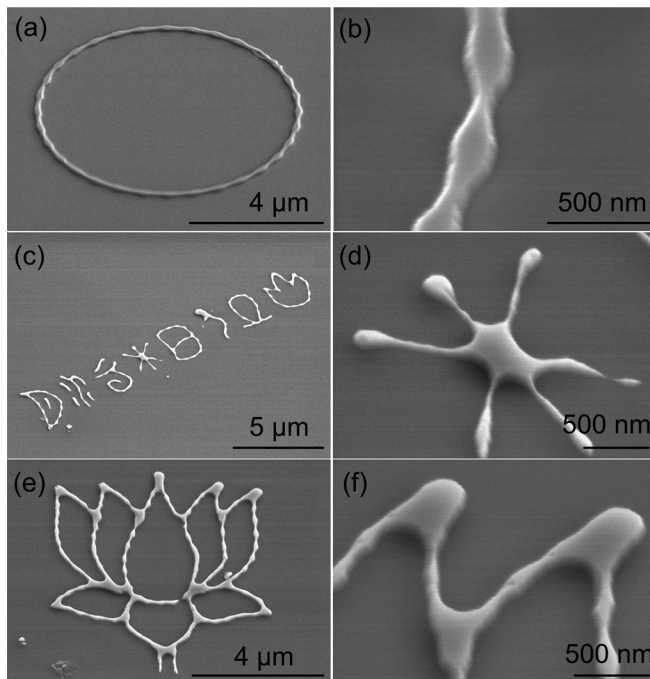

FIG. 6. SEM images of complex silicon oxide nanostructures fabricated via TBN. (a) Ring structure with 6 μm diameter. (b) Zoomed-in view of a section of ring structure. (c) Set of ancient Chinese characters. (d) Zoomed-in view of a single character. (e) Nanostructure in the shape of a lotus flower. (f) Zoomed-in view of a section of the lotus flower.
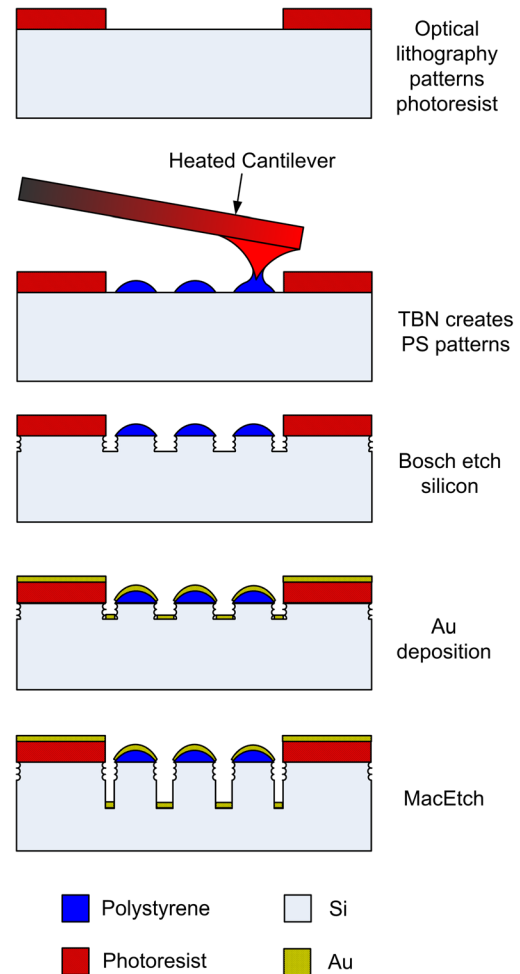

FIG. 7. (Color online) Schematics showing the major steps for transferring PS nanostructures to a gold film and creating silicon nanostructures by TBN and MacEtch.

we fabricated a 9 μm square array of a photoresist pattern using conventional micro optical lithography to assist the MacEtch process. The micropatterning process ensured that the extent of the Gold layer, used as the MacEtch catalyst, could be limited to a finite area for improved control over vertical etching of high-aspect ratio features compared to MacEtch of a sample with no micropatterning of gold films. Limiting the gold within a small area allows the MacEtch solution to penetrate through the sides of the micropatterned region to etch the oxidized silicon more uniformly. If gold is not limited within a small area, the MacEtch solutions will reach the oxidized silicon on the peripheral region much easier than the oxidized silicon in the middle, resulting in nonuniform etching. Next, a heated AFM tip deposited PS nanopatterns on the silicon within the 9 μm hole. We then etched silicon via the Bosch process consisting of alterative steps of passivation and etching to form a shallow silicon structure having a profile amenable to gold lift-off. After Bosch etching, we evaporated a 35 nm thick gold layer onto the sample. Finally, we dipped the sample into a MacEtch solution to produce the silicon nanostructures. MacEtch was performed for a period of 25 min at room
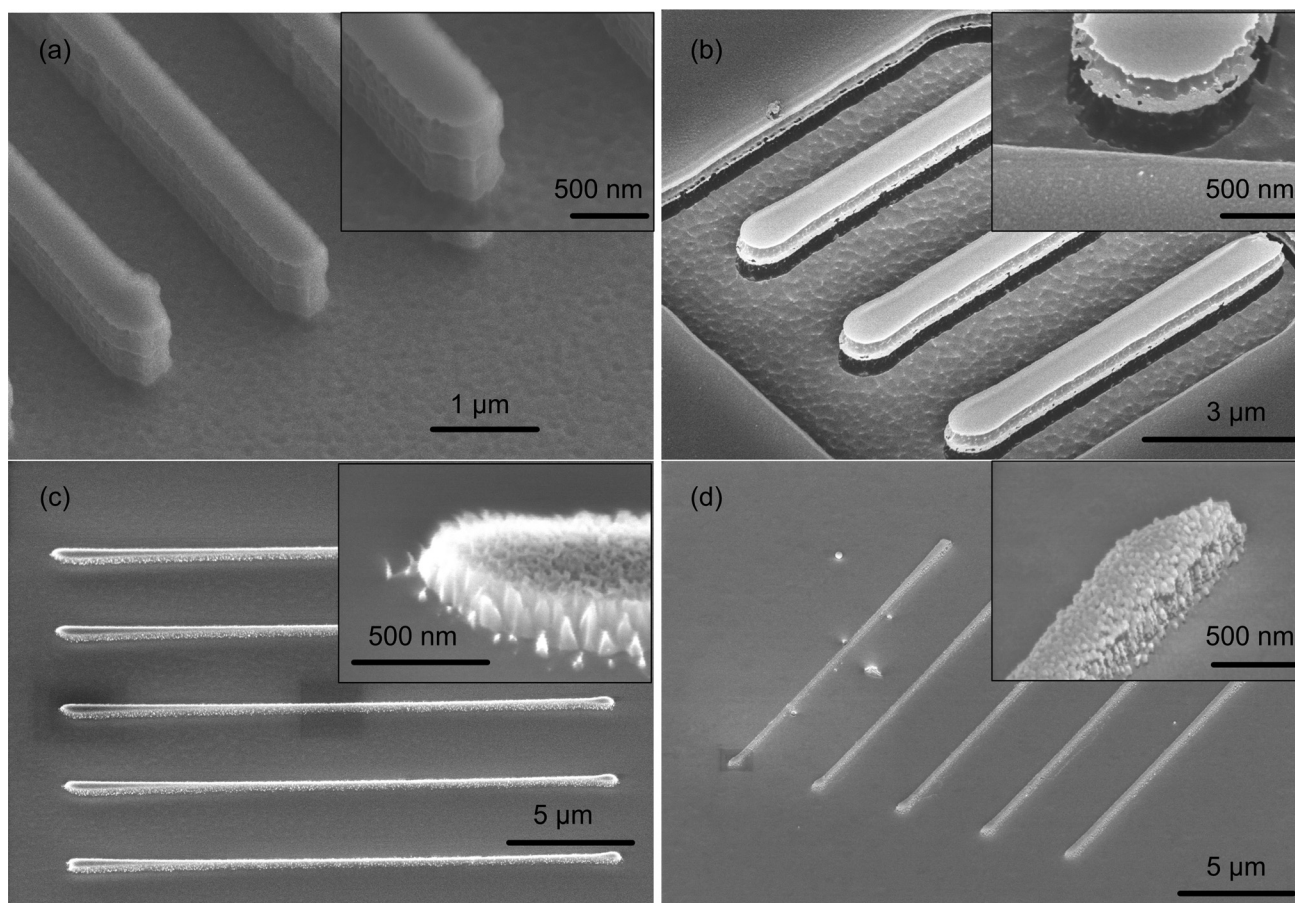
FIG. 8. Comparison of Bosch silicon etch and RIE nitride etch. (a) SEM image of silicon fins after Bosch etch using PS nanostructures directly as an etching mask. (b) SEM image of silicon fins after 35 nm thick gold evaporation. The gold film on the sidewall of the fin is separated from the gold film on the bottom. (c) SEM image of 250 nm thick SiNx fins after 5 min RIE using PS nanostructures as etch mask. (d) SEM image of the SiNx fins after 35 nm thick gold evaporation. The gold film on the fin sidewall is contiguous with the gold film on the bottom, blanketing the entire SiNx fin and, thus, preventing the MacEtch from occurring.

temperature in a solution of HF, hydrogen peroxide (H_2O_2), and ethanol (EtOH), with a volumetric ratio of 1:2:2, respectively (molar concentration of $[HF] = 5.75$ M, $[H_2O_2] = 3.88$ M, $[EtOH] = 6.86$ M).

Figure 8 compares the results of using Bosch etch to the results of using normal RIE before the MacEtch step. Figure 8(a) shows the silicon fin structures after Bosch silicon etch for four cycles using PS patterns as mask, and Fig. 8(b) shows the results after evaporating 35 nm thick gold film. The subset image of Fig. 8(b) shows that the gold film on the bottom is separated from the gold film on the sidewall of the fin. Figure 8(c) shows silicon nitride nanostructures fabricated using TBN. We first deposited PS nanostructures using the heated AFM tip on top of a 250 nm thick silicon nitride layer prepared by plasma enhanced chemical vapor deposition. Then, we etched the silicon nitride using PS nanostructures as etch mask in RIE for 5 min. The RIE conditions are 35 mTorr pressure, 90 W RF power, and 60 sccm flow of CHF_3 gas. Figure 8(d) shows the silicon nitride structure after evaporation of a 35 nm thick gold layer. The subset image inside Fig. 8(d) shows that the gold film on the sidewall is connected with the gold film on the substrate surface, thereby covering the

entire silicon nitride structure and preventing controlled MacEtch from proceeding.

Figure 9 shows the SEM images of various silicon nanostructures fabricated using TBN and MacEtch. Figures 9(a) and 9(b) show an array of six silicon fin structures, where each fin is 6 μm in length, 400 nm in width, and 500 nm in thickness. The lower part of the silicon fin fabricated by MacEtch is smoother than the upper part of the silicon fin structure formed by Bosch silicon etch. With optimized MacEtch conditions, the sidewall roughness of the silicon nanowires fabricated by MacEtch can be as low as 2 nm.[29] Figures 9(c) and 9(d) show a lotus flower shaped structure that is about 4 μm in size and 500 nm in thickness. Figures 9(e) and 9(f) show an array of 3×3 vertical silicon nanowires (Si NW) with diameter about 500 nm for each Si NW.

Figure 10 shows many arrays of Si NWs with different spacing and matrix sizes. Figure 10(a) shows an overview of 20 vertical arrays of Si NWs, within each square cell. All the Si NWs are 500 nm in diameter and 8 μm in height. Figure 10(b) shows a 3×3 array of vertical Si NWs with a spacing of 2 μm. Figure 10(c) shows a 4×4 array of vertical Si NWs and each nanowire is spaced by 1.5 μm. Figure 10(d) shows a 6×6 array of vertical Si NWs and the spacing is 1 μm.
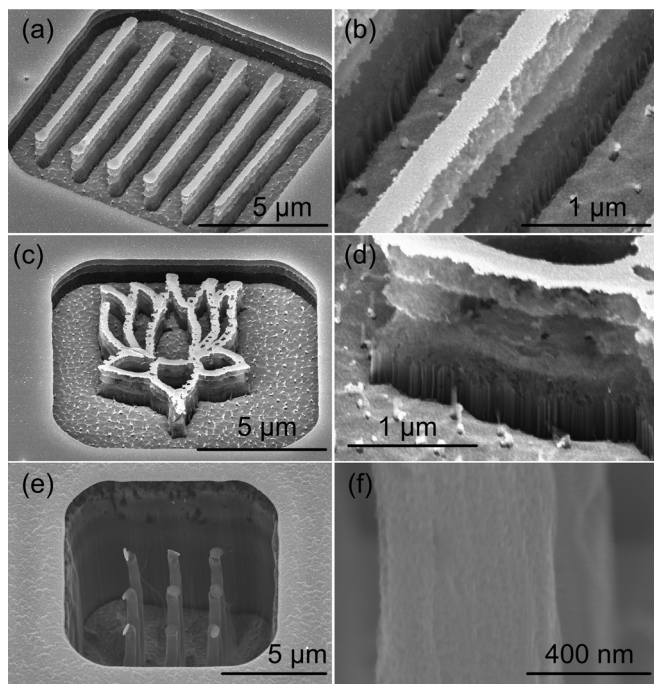
Fig. 9. SEM images of different types of structures fabricated by TBN and MacEtch. (a) Array of six fins with 500 nm thick silicon. (b) Zoomed-in view of a single fin with bottom part silicon formed by MacEtch smoother than top part silicon formed by Bosch etch. (c) Lotus flower shape with bottom part silicon formed by MacEtch and top part silicon formed by Bosch Etch. (d) Zoomed in view of the profile of the structure of (c). (e) Array of 9 μm tall vertical Si nanostructures. (f) Zoomed-in view of one Si nanostructure showing the smoothness of the sidewall rendered by MacEtch.

The Si NWs stick to adjacent NWs and form bundles due to the surface tension of wet liquids when Si NWs are packed very closely.

III. DISCUSSION

There are three criteria for qualify a polymer material to serve as an etching mask. First, the polymer must survive through the wet chemical etching or reactive ion etching that follows the polymer deposition. Second, the polymer should be removed easily in order to limit contamination. Third, the polymer must adhere to the substrate well. PS satisfies all the above criteria. We found 60 nm thick PS patterns deposited by the heated AFM tip can survive for 2 min in a standard Bosch etch process, 5 min of CHF_3 RIE (60 sccm gas flow, 35 mTorr pressure, 90 W RF power), and more than 2 min in BHF wet etching. Moreover, PS can easily be removed by acetone or oxygen plasma RIE, both of which are very common processes in nanofabrication and will not result into contamination.

TBN offers many advantages over other nanolithography methods. In terms of cost, TBN can be performed using equipment that is much less expensive than equipment used by EBL or FIB. TBN can fabricate arbitrary shapes of nanostructures while nanoimprint lithography requires a mask to be fabricated before imprinting. TBN can also fabricate nanostructures onto a non-flat substrate. Finally, the AFM
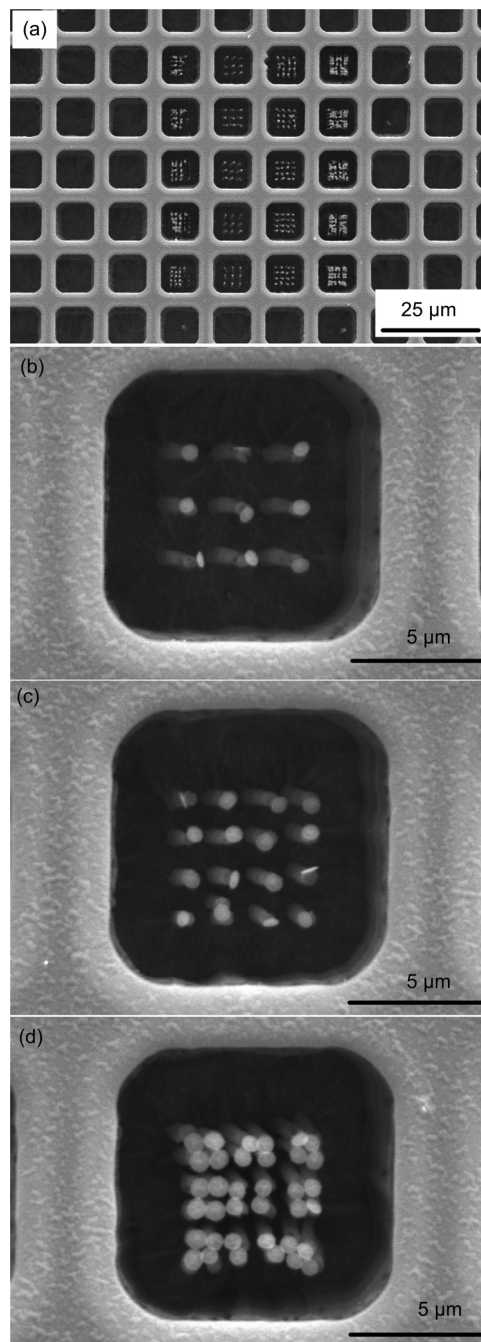

Fig. 10. High aspect ratio vertical silicon nanostructures fabricated using TBN and MacEtch. (a) Overview of many arrays of smooth vertical silicon nanostructures. (b) Array with 2 μm spacing. (c) Array with 1.5 μm spacing. (d) Array with 1 μm spacing. These silicon nanostructures can form bundles when the spacing is small.

function of TBN can be used to perform metrology during fabrication.

IV. CONCLUSIONS

We have presented a TBN technique that enables fabrication of silicon and silicon oxide through one step of etching, which makes it compatible with existing nanofabrication methods and suitable for device nanofabrication. PS nanostructures deposited from a heated AFM cantilever serve as

etching mask and transfer the PS nanostructures to silicon or silicon oxide through etching. We demonstrated arbitrary shapes of silicon and silicon oxide nanostructure such as rings, curved lines, and a lotus flower. We also demonstrated the integration of TBN with both conventional wet etching and MacEtch. Moreover, due to the additive nature of our TBN method, it results in much less contamination than other nanolithography techniques that require spincoat of resist.

ACKNOWLEDGMENTS

[1]D. M. Eigler and E. K. Schweizer, Nature **344**, 524 (1990).

[2]H. Gobel and P. Vonblanckenhagen, J. Vac. Sci. Technol. B **13**, 1247 (1995).

[3]J. A. Dagata, Science **270**, 1625 (1995).

[4]D. Hwang, S. G. Ryu, N. Misra, H. Jeon, and C. P. Grigoropoulos, Appl. Phys. A **96**, 289 (2009).

[5]R. D. Piner, J. Zhu, F. Xu, S. H. Hong, and C. A. Mirkin, Science **283**, 661 (1999).

[6]P. E. Sheehan, L. J. Whitman, W. P. King, and B. A. Nelson, Appl. Phys. Lett. **85**, 1589 (2004).

[7]X. Q. Chen, H. Yamada, T. Horiuchi, K. Matsushige, S. Watanabe, M. Kawai, and P. S. Weiss, J. Vac. Sci. Technol. B **17**, 1930 (1999).

[8]I. W. Rangelow, J. Voigt, and K. Edinger, J. Vac. Sci. Technol. B **19**, 2723 (2001).

[9]R. V. Martinez, J. Martinez, and R. Garcia, Nanotechnology **21**, 245301 (2010).

[10]M. Villarroya, F. Perez-Murano, C. Martin, Z. Davis, A. Boisen, J. Esteve, E. Figueras, J. Montserrat, and N. Barniol, Nanotechnology **15**, 771 (2004).

[11]J. Martinez, R. V. Martinez, and R. Garcia, Nano. Lett. **8**, 3636 (2008).

[12]S. Minne, H. Soh, P. Flueckiger, and C. Quate, Appl. Phys. Lett. **66**, 703 (1995).

[13]K. Matsumoto, M. Ishii, K. Segawa, Y. Oka, B. Vartanian, and J. Harris, Appl. Phys. Lett. **68**, 34 (1996).

[14]R. Held, T. Vancura, T. Heinzel, K. Ensslin, M. Holland, and W. Wegscheider, Appl. Phys. Lett. **73**, 262 (1998).

[15]M. Fuechsle, J. A. Miwa, S. Mahapatra, H. Ryu, S. Lee, O. Warschkow, L. C. L. Hollenberg, G. Klimeck, and M. Y. Simmons, Nat. Nanotechnol. **7**, 242 (2012).

[16]L. Pellegrino, E. Bellingeri, I. Pallecchi, A. Siri, D. Marre, and A. Chincarini, J. Electroceram. **13**, 331 (2004).

[17]G. P. Lopinski, D. D. M. Wayner, and R. A. Wolkow, Nature **406**, 48 (2000).

[18]B. Klehn and U. Kunze, J. Appl. Phys. **85**, 3897 (1999).

[19]D. Pires, J. L. Hedrick, A. De Silva, J. Frommer, B. Gotsmann, H. Wolf, M. Despont, U. Duerig, and A. W. Knoll, Science **328**, 732 (2010).

[20]M. Rolandi, C. F. Quate, and H. J. Dai, Adv. Mater. **14**, 191 (2002).

[21]D. A. Weinberger, S. G. Hong, C. A. Mirkin, B. W. Wessels, and T. B. Higgins, Adv. Mater. **12**, 1600 (2000).

[22]L. Pellegrino, Y. Yanagisawa, M. Ishikawa, T. Matsumoto, H. Tanaka, and T. Kawai, Adv. Mater. **18**, 3099 (2006).

[23]K. S. Salaita, S. W. Lee, D. S. Ginger, and C. A. Mirkin, Nano. Lett. **6**, 2493 (2006).

[24]P. Avouris, T. Hertel, and R. Martel, Appl. Phys. Lett. **71**, 285 (1997).

[25]J. R. Felts, S. Somnath, R. H. Ewoldt, and W. P. King, Nanotechnology **23**, 215301 (2012).

[26]S. Somnath, E. A. Corbin, and W. P. King, IEEE Sen. J. **11**, 2664 (2011).

[27]Z. P. Huang, N. Geyer, P. Werner, J. de Boor, and U. Gosele, Adv. Mater. **23**, 285 (2011).

[28]X. L. Li, Curr. Opin. Solid State Mater. Sci. **16**, 71 (2012).

[29]K. Balasundaram *et al.*, Nanotechnology **23**, 305304 (2012).